Süfke Finn (Orcid ID: 0000-0001-5271-1099)

Pöppelmeier Frerk (Orcid ID: 0000-0003-4050-2550)

Koutsodendris Andreas (Orcid ID: 0000-0003-4236-7508)

Blaser Patrick (Orcid ID: 0000-0001-8102-9777)

Gutjahr Marcus (Orcid ID: 0000-0003-2556-2619)

Lippold Jörg (Orcid ID: 0000-0003-1976-5065)

Constraints on the northwestern Atlantic deep water circulation from $^{231}Pa/^{230}Th$ during the last 30,000 years

Finn Süfke[1], Frerk Pöppelmeier[1], Tyler Jay Goepfert[2], Marcel Regelous[3], Andreas Koutsodendris[1], Patrick Blaser[1], Marcus Gutjahr[2], and Jörg Lippold[1]

[1] Heidelberg University, Institute of Earth Sciences, Heidelberg, Germany

[2] GEOMAR Helmholtz Centre for Ocean Research Kiel, Kiel, Germany

[3] FAU Erlangen-Nürnberg, GeoZentrum Nordbayern, Erlangen, Germany

Corresponding author: Finn Süfke (finn.suefke@geow.uni-heidelberg.de)

Key Points:

- Four new $^{231}Pa/^{230}Th$ records form a depth transect in the northwestern Atlantic in millennial scale resolution back to 30 ka
- Combined records resolve millennial scale deep water variabilities like YD, B/A, HS1, LGM and HS2
- Timing and magnitude of record variations are in line with the well-known Bermuda Rise record with exception of the LGM

This article has been accepted for publication and undergone full peer review but has not been through the copyediting, typesetting, pagination and proofreading process which may lead to differences between this version and the Version of Record. Please cite this article as doi: 10.1029/2019PA003737

Abstract

Global climatic changes during the last Glacial and Deglacial have been related to variations of the Atlantic Meridional Overturning Circulation (AMOC). Here, we present new and refined $^{231}Pa/^{230}Th$ down-core profiles extending back to 30 ka BP from the northwestern Atlantic along the Atlantic Deep Western Boundary Current (DWBC), which is the main component of the southward deep backflow of the AMOC. Besides the well-known Bermuda Rise records, available high-resolution $^{231}Pa/^{230}Th$ data in the northwestern Atlantic are still sparse. Our new records along with reconstructions of deep water provenance from Nd isotopes constrain the timing and magnitude of past changes in AMOC from an additional northwestern Atlantic region forming a depth transect between 3000 and 4760 m water depth. Our extended and improved dataset confirms the weakening of the AMOC during deglacial cold spells such as Heinrich Event 1 and the Younger Dryas interrupted by a reinvigoration during the Bølling-Allerød interstadial as seen in the prominent $^{231}Pa/^{230}Th$ records from the Bermuda Rise. However, in contrast to the Bermuda Rise records we find a clearly reduced circulation strength during the Last Glacial Maximum in the deep Atlantic.

1. Introduction

Deep water formation in and around the North Atlantic represents an important feature of Earth's climate system, since it redistribute water masses between the surface and the deep ocean as well as between the northern and southern hemisphere. Accordingly, reconstructions of the Atlantic Meridional Overturning Circulation (AMOC) by means of various proxies and methods have been carried out extensively in the last decades in order to determine its behavior under very different past climatic boundary conditions (e.g. McManus et al., 2004; Curry and Oppo, 2005; Lynch-Stieglitz, 2017). Today, the majority of the deep western Atlantic basin is occupied by North Atlantic Deep Water (NADW) which is transported southwards primarily by the Atlantic Deep Western Boundary Current (DWBC) (Fig. 1; Johnson, 2008; Rhein et al., 2015). North Atlantic Deep Water is underlain by Southern Sourced Water (SSW) which reaches into the deep North Atlantic up to 40°N (Johnson, 2008). The modern distribution of these water masses is clearly reflected by nutrient concentrations such as phosphate (Garcia et al., 2014) or physical properties such as salinity and potential temperature (Broecker et al., 1985, Zweng et al., 2013; Locarini et al., 2013). The distribution of these water masses changed on millennial scales and has been reconstructed with nutrient-based proxies such as $\delta^{13}C$ and Cd/Ca (e.g. Keigwin, 2004; Curry

and Oppo, 2005; Oppo et al., 2018). An alternative approach for the identification of different water masses is the radiogenic neodymium isotope proxy (denoted as εNd). Neodymium isotopes are extracted from the authigenic phases of bulk sediments, foraminifera or fish teeth on which ideally the water mass Nd isotopic signature have been imprinted (e.g. Gutjahr et al., 2008; Piotrowski et al., 2005; Blaser et al., 2016; Howe et al., 2016). Different reconstructions showed that during the Last Glacial Maximum (LGM) as well as during short northern hemispheric cold spells such as Heinrich Stadials 1 and 2 (HS1 and HS2) and the deglacial Younger Dryas (YD), the balance of these water masses shifted towards a predominance of SSW filling most of the deep western Atlantic reaching north as far as 50-60°N (Curry and Oppo, 2005; Marchitto and Broecker, 2006; Roberts et al., 2010; Gutjahr and Lippold, 2011). However, recent studies suggested the presence of a deep northern sourced water mass in the northwestern Atlantic also during the LGM as derived from stable carbon isotopes (Keigwin and Swift, 2017) and εNd data (Pöppelmeier et al., 2018; Howe et al., 2016).

Alongside reconstructions of past water masses distribution the knowledge of the past overturning strength from sensitive locations and different water depths is of equal importance. Reconstructions of bottom water circulation at the Blake Bahama Outer Ridge (BBOR; Fig. 1) using sortable silt suggested a reduced circulation during the LGM below 3000 m water depth, but with a strong shallow circulation cell above (Evans and Hall, 2008). These authors further suggest stronger circulation in the abyssal (>4000 m) northwestern Atlantic, which they interpret as intensified SSW inflow. Sortable silt is a valuable proxy for reconstructing local bottom currents (McCave et al., 1995; McCave et al., 2017) but provides less information about the large-scale AMOC. For such large-scale AMOC reconstructions, the kinematic circulation strength proxy $^{231}Pa/^{230}Th_{excess}$ is widely applied in the Atlantic (McManus et al., 2004; Lippold et al., 2012a; Yu et al., 1996; Ng et al., 2018). Both, ^{231}Pa and ^{230}Th, are daughter isotopes from the radioactive decay of the uranium isotopes ^{235}U and ^{234}U, respectively. Uranium (and its isotopic composition) is homogeneously dissolved in the world ocean due to the long residence time in the order of 400 ka (Henderson and Anderson, 2003). Accordingly, the production of both daughter isotopes is of a constant activity ratio (0.093; hereafter 'production ratio'). In contrast to uranium, protactinium and thorium are highly particle reactive, leading to short oceanic residence times of 100-200 and 10-40 years, respectively (Henderson and Anderson, 2003). Due to the slightly longer residence time of protactinium (roughly the time it takes for NADW to reach the Southern Ocean; Yu et al.,

1996), ^{231}Pa and ^{230}Th are fractionated in dependence of the circulation strength (i.e. changes in AMOC intensity). Hence, low sedimentary ^{231}Pa/^{230}Th values today in the deep Atlantic reflect strong NADW advection (meridional ^{231}Pa export to the Southern Ocean), while higher values are consistent with a weaker AMOC state (Luo et al., 2010; McManus et al., 2004).

In the Southern Ocean, ^{231}Pa is preferentially scavenged from the water column into sediments due to its high affinity to particles consisting of biogenic opal (Chase et al., 2003). From this observation, a critical view on the usage of ^{231}Pa/^{230}Th as a circulation proxy arose, since ^{231}Pa/^{230}Th might be strongly linked to particle fluxes and their compositions (Chase et al., 2003). For regions with high particle fluxes and characteristic particle compositions (e.g. the Southern Ocean) or weak ocean circulation (e.g. the Pacific) this effect seems to control sedimentary ^{231}Pa/^{230}Th ratios (Anderson et al., 1983; Chase et al., 2003; Hayes et al., 2013; Costa et al., 2017). In contrast, in the western Atlantic, with its relatively moderate particle fluxes and a pronounced AMOC, ^{231}Pa is effectively exported from the North to South Atlantic by advection as derived from a ^{231}Pa deficit of at least 26 % (Deng et al., 2018) (a former study by Yu et al. (1996) mentioned up to 50 %) supporting the applicability of ^{231}Pa/^{230}Th as a circulation proxy in the Atlantic.

Previous studies using the ^{231}Pa/^{230}Th proxy have concluded that a strong circulation of the North Atlantic prevailed during the Holocene (Hoffmann et al., 2018) and pronounced weakenings of AMOC strengths occurred during past cold phases (McManus et al., 2004; Bradtmiller et al., 2014; Gherardi et al., 2009; Ng et al., 2018; Lippold et al., 2016). Nevertheless, a clear picture of the vertical structure of the deglacial circulation and the evolution of AMOC is still lacking, in particular due to insufficient spatial and temporal proxy coverage.

Here we present four new high-resolution ^{231}Pa/^{230}Th down-core profiles forming a depth transect at the BBOR (3000 to 4760 m; Fig. 1) spanning the last 30 ka. The BBOR is a well-studied location (e.g. Keigwin, 2004; Evans and Hall, 2008) in the direct flow path of the DWBC that allows for the investigation of advection rates depending on the water depth. Additionally, we provide three updated and improved records from a prior study (Lippold et

al., 2016). With these new records from the deep BBOR we are able to reconstruct the evolution and changes in AMOC strength in greater detail.

2. Materials and Methods

2.1. Setting and age model

We analyzed $^{231}Pa/^{230}Th$ from ODP Leg 172 Sites 1059, 1060, 1061 and 1062 back to 30 ka. Sites 1059, 1060 and 1061 are located on the crest of the Blake Outer Ridge, which is formed by drift sediments (Keigwin and Jones, 1994), while Site 1062 is located further south on the Bahama Outer Ridge (Fig. 1). The four sites form a depth transect from 3000 to 4760 m water depth. In addition, we improved the $^{231}Pa/^{230}Th$ records (partly re-analyzed and re-calibrated, see Table S5) of KNR140 12JPC (hereafter 12JPC) on the BBOR and cores GeoB1515-1 and GeoB1523-1 from the Ceara Rise in the equatorial western Atlantic (Lippold et al., 2016). Age models for Sites 1059 to 1062 are provided by Pöppelmeier et al. (2019) and are based on the correlation of carbonate concentration for Site 1059 and 1062 (Grützner et al., 2002) to neighboring cores KNR140 GGC39 (Keigwin and Schlegel, 2002) and KNR31 GPC9 (Keigwin and Jones, 1994), respectively. Additionally, the age model consists of 12 ^{14}C dates on Site 1060, two dates on Site 1062 and four recalibrated ^{14}C dates on Site 1059 (Hagen and Keigwin, 2002, Pöppelmeier et al., 2019). We further present new age models for GeoB1515-1 and GeoB1523-1 from the Ceara Rise, which have been improved by recalibrated ^{14}C dates and one new ^{14}C date for GeoB1515-1. This new ^{14}C date was measured at the LARA laboratory at the University of Bern, Switzerland (Gottschalk et al., 2018). We used the CALIB 7.1 online tool tied to the Marine13 curve (Reimer et al., 2013) for calibration of all ^{14}C dates with the standard 400-year reservoir age correction.

2.2. Analytical procedure for Pa, Th and U isotope measurements

Sediment samples were analyzed for the radioisotopes ^{230}Th, ^{231}Pa, ^{232}Th, ^{234}U, and ^{238}U. Purification and separation of the elements followed the protocol described in Süfke et al. (2018). Before chemical treatment samples were spiked with ^{233}Pa, ^{229}Th and ^{236}U. The short-lived ^{233}Pa isotope ($t_{1/2}$= 27 d) was milked from a ^{237}Np solution using the procedure described by Regelous et al. (2004). The ^{233}Pa spike was calibrated against the reference material UREM-11 (Süfke et al., 2018) and an internal pitchblende standard (Fietzke et al., 1999). Protactinium isotopes were measured using an Element 2 HR-ICP-MS in the Institute of Earth Sciences at Heidelberg University and a Neptune Plus MC-ICP-MS in the

Geozentrum Nordbayern at the Friedrich–Alexander University in Erlangen equipped with a retarding potential quadrupole filter. Uranium and thorium isotopes were measured with two Neptune Plus MC-ICP-MS at GEOMAR Helmholtz Centre for Ocean Research in Kiel and at the Geozentrum Nordbayern in Erlangen.

A detrital correction ($^{238}U/^{232}Th$) of 0.55, in agreement to overall minima of bulk $^{238}U/^{232}Th$, was applied to the measured activities of ^{231}Pa and ^{230}Th in accordance with the typical lithogenic activity ratio for $^{238}U/^{232}Th$ of 0.5 to 0.6 (Henderson and Anderson, 2003) in the western Atlantic. The lithogenic $^{238}U/^{232}Th$, and hence the detrital correction on the calculation of $^{231}Pa/^{230}Th$, may vary with time (Missiaen et al., 2018) in particular during times of high detrital and/or authigenic contributions. One control parameter for a potentially changing detrital factor is given by the $^{230}Th_{xs0}/^{232}Th$ ratios (Missiaen et al., 2018). Throughout the glacial to deglacial parts of the records, the $^{230}Th_{xs0}/^{232}Th$ activity ratios are relatively constant, pointing to a stable detrital phase , but shows strong increases with the onset of the Holocene (Fig. S1). However, the Holocene sections of our $^{231}Pa/^{230}Th$ records are insensitive to changes in the detrital correction (Fig. S2). Furthermore, X-Ray Fluorescence (XRF) data (cf. section 2.3. and 3.2.) support a uniform detrital sediment composition throughout the complete records (Fig. S4). Hence, we used a constant detrital correction of 0.55 that has also previously been used for Site 12JPC (Lippold et al., 2016). The ingrowth of ^{231}Pa and ^{230}Th from authigenic uranium was calculated and corrected as described by Henderson and Anderson (2003). Finally, ^{231}Pa and ^{230}Th excess concentrations were decay corrected to the time of deposition. All individual isotope concentrations are provided in the supplement (Tables S1-S6).

2.3. Biogenic opal and major elements

As well as the measurements of $^{231}Pa/^{230}Th$, we analyzed the content of biogenic opal in the sediments. High fluxes of biogenic opal may increase $^{231}Pa/^{230}Th$ ratios independently of the circulation strength, due to the high affinity of ^{231}Pa to it (e.g. Chase et al., 2002, 2003; Rutgers van der Loeff et al., 2016). Opal concentrations were analyzed by automated leaching following the procedure described by Müller and Schneider (1993). Furthermore, we measured the bulk sediment content of Al, Si, Ti, Fe and K of discrete samples (Table S7) with a fourth generation Avaatech XRF core scanner at the Institute of Earth Sciences at

Heidelberg University, using a 10 kV Rh anode X-ray tube without a filter, a 1000 mA current (500 mA for Site 1060), and a counting time of 30 seconds.

2.4. Selection criteria for compilation of existing $^{231}Pa/^{230}Th$ profiles from the West Atlantic for comparison

In order to provide a comprehensive $^{231}Pa/^{230}Th$ based picture of the deep AMOC evolution in the western Atlantic sector we compiled new and existing records from this basin. We only used sites from the western basin of the Atlantic since records from the eastern basin show noticeably different features and deglacial evolution due to different circulation regimes in both basins (Bradtmiller et al., 2007; Gherardi et al., 2009; Howe et al., 2017; Ng et al., 2018; Lippold et al., 2012b). For this compilation we excluded sites which are located on or near the Mid-Atlantic-Ridge (MAR) in order to avoid potential effects of hydrothermal activity on regional $^{231}Pa/^{230}Th$ (Hayes et al., 2015a; Pavia et al., 2018; Lund et al., 2019) which are not yet satisfyingly resolved (Bradtmiller et al., 2007, Lippold et al., 2016, Gherardi et al., 2009). We further excluded sites where records are not continuous from the LGM to the Holocene or from which the original authors consider specific time intervals as questionable (Gherardi et al., 2009; Lippold et al., 2011). Overall, we thus compiled two cores from the Bermuda Rise (McManus et al., 2004; Lippold et al., 2009), five from the BBOR (this study, Lippold et al., 2016) and five from the central/equatorial western basin (Bradtmiller et al., 2007; Lippold et al., 2016; Ng et al., 2018) which fulfill our criteria (Fig. 1). In the further interpretation we combined the two cores GeoB1523-1 (Lippold et al., 2016) and EW9209-3JPC (Ng et al., 2018) to a single record since both sites are situated at the same water depth and nearly the same location.

3. Results

3.1. $^{231}Pa/^{230}Th$

All new records show a similar millennial scale variability closely following the prominent Bermuda Rise record (McManus et al., 2004; Lippold et al., 2009; Fig. 2). Youngest $^{231}Pa/^{230}Th$ values are consistently low (between 0.053 and 0.060) indicative of strong ^{231}Pa export that was established during the early Holocene (< 10 ka) (Figs. 2, 3). Pronounced variability during the deglaciation including the prominent climatic episodes YD, Bølling-Allerød (B/A) and HS1 is present in all new records, except for the re-evaluated Site 12JPC, which shows less variability during the YD and B/A events.

The $^{231}Pa/^{230}Th$ ratios from all deep cores follow a general temporal evolution from high glacial values towards low values during the early Holocene, only disrupted by a prominent short and rapid decrease during the B/A (almost reaching Holocene values) and again glacial-like values during the short period of the YD. The decrease in $^{231}Pa/^{230}Th$ during the B/A of the shallowest Site 1059 (2984 m) is less pronounced and/or exhibits a different timing. During HS1 all records show generally high $^{231}Pa/^{230}Th$ values (but below the production ratio) ranging from 0.072 to 0.086 (average = 0.081 ± 3.6 %), in agreement with abyssal $^{231}Pa/^{230}Th$ records of the northwestern Atlantic (McManus et al., 2004; Lippold et al., 2009; Ng et al., 2018).

The new $^{231}Pa/^{230}Th$ values from the LGM are slightly lower (average = 0.073 ± 4.2 %) than those during HS1. This subtle difference is in contrast to the prominent Bermuda Rise record that features significantly lower LGM values (Fig. 2; McManus et al., 2004). At the BBOR, the lowest LGM values were recorded in the shallowest Site 1059, whereas LGM values from Sites 1060 and 1061 are nearly indistinguishable from values observed during HS1.

While $^{231}Pa/^{230}Th$ ratios of Site 1059 exhibit no distinct peak during HS2, the deeper BBOR cores display generally higher variability during this period and values as high as during HS1,

including few values exceeding the production ratio of 0.093. In particular, Site 1060 shows a double peak feature similar to the record at ODP Site 1063 (Lippold et al., 2009).

3.2. Opal and major elemental abundances

Low preserved opal concentrations below 4 % were measured in all presented BBOR cores (Fig. 2). Further, a higher opal content should be detectable by increased Si/Al ratios (McManus et al. 2004) but are not present in the new XRF records from the BBOR (Fig. S4). In addition to the Si/Al ratio, we used other elemental ratios obtained by XRF for analyzing the provenance and major composition of the sedimentary phase. Ratios of Ti/Al, K/Al, K/Ti and Ti/Fe show little variation throughout the entire records (Fig. S4), pointing to an invariable detrital phase (Rothwell and Croudace, 2015), which in turn supports the selection of a constant detrital correction as outlined in section 2.2.

4. Discussion

4.1 Potential primary particle influences on $^{231}Pa/^{230}Th$

As seen from its high $^{231}Pa/^{230}Th$, ^{231}Pa exported southward via NADW ends in the sediments of the Southern Ocean (Rutgers van der Loeff et al., 2016) due to the opal-dominated particle flux in this region (Walter et al., 1997; Chase et al., 2003; Anderson et al., 2009). Therefore, the role of particle flux and particle composition on controlling sedimentary $^{231}Pa/^{230}Th$ besides ocean circulation is emphasized (Chase et al., 2002; Geibert and Usbeck, 2004). While biogenic opal has not been found to be a significant scavenging phase in the modern north Atlantic ocean (Hayes et al., 2015b) we also exclude opal as a major driver of $^{231}Pa/^{230}Th$ at the BBOR for the past. Preserved opal concentrations are constantly low at all BBOR Sites during the last 30 ka (even in the presence of high $^{231}Pa/^{230}Th$ variability). Comparing $^{231}Pa/^{230}Th$ and opal concentrations from all sites used for this study (McManus et al., 2004; Bradtmiller et al., 2007; Lippold et al., 2009, 2016; Ng et al., 2018) no persuasive correlation is present and opal concentrations are always below 5% (Fig. S3).

Besides opal, authigenic Fe and/or Mn hydroxides are potential strong scavengers of ^{231}Pa and ^{230}Th (Hayes et al., 2015b). Indeed, along the GA03 GEOTRACES North Atlantic Transect (Hayes et al., 2015a) K_d values of MnO_2 and $Fe(OH)_3$ have been estimated at magnitudes higher than for lithogenic particles or $CaCO_3$ (Hayes et al., 2015b). This effect was observed emanating from hydrothermal plumes of the MAR (Hayes et al., 2015b).

However, due to the large distance between the MAR and the BBOR, scavenging by Mn/Fe phases originating from the MAR can be considered as negligible. Furthermore, increased scavenging of ^{231}Pa and ^{230}Th by MnO_2 has been reported in bottom water particles off the Mauritanian margin (Hayes et al., 2015b). In contrast to the BBOR the Mauritanian margin is a region of high upwelling intensity. There, ^{231}Pa can be scavenged by MnO_2 coatings formed from redox cycling from the respiration of high contents of organic matter (Hayes et al., 2015b), but such conditions have not been observed at the BBOR. Although the mobility of Fe and Mn may have been quite different between glacial and interglacial conditions due to lower oxygenation, effects of increased ^{231}Pa and/or ^{230}Th scavenging are rather expected under very sluggish circulation regimes such as the Pacific (Korff et al., 2016)

Alongside particle composition the sheer amount of particles may also increase ^{231}Pa/^{230}Th, in particular at ocean margins (so-called boundary scavenging; Anderson et al., 1983; Hayes et al., 2015a). Increased ^{231}Pa/^{230}Th have been found from the high accumulating and organic rich sediments off the coast of West Africa (Christl et al., 2010; Lippold et al., 2012b; Scholten et al., 2008; Hayes et al., 2015a), however still overprinted by an AMOC signal in their temporal evolution (Lippold et al., 2012b). The effects of boundary scavenging and increased particle fluxes at the high productivity upwelling regions off West Africa are not comparable with the BBOR as discussed before.

On the other hand, the effect of bottom scavenging due to the occurrences of nepheloid layers (Hayes et al., 2015a) may represent an additional sink for ^{231}Pa and ^{230}Th at the sea floor. A first simple representation of bottom scavenging in a ^{231}Pa/^{230}Th enabled model (Rempfer et al., 2017) did not yield a disturbed relationship between overturning strength and ^{231}Pa/^{230}Th on the larger spatial and temporal scales in the Atlantic. The implementation of bottom scavenging in the model, however, was global. Nepheloid layers were assumed to appear in all bottom grid cells with the thickest layers in the deepest water depths. Accordingly, the model is able of capturing a basin wide relation rather than a local influence. Temporally variable occurrences of local and regional nepheloid layers may be able to influence a ^{231}Pa/^{230}Th profile to a certain extent possibly increasing sedimentary ^{231}Pa/^{230}Th ratios (Deng et al., 2014). Today, parts of the northwestern Atlantic have been found to be covered by nepheloid layers (Stahr and Sanford, 1999; Gardner et al., 2018). Effects of nepheloid layers on Nd isotopes have been reported from the BBOR e.g. by offsets found between core tops and seawater Nd isotopic compositions and by the manifestation of unradiogenic

anomalies in Nd isotopic signatures attenuating as a function of distance to the presence of strong benthic nepheloid layers (Pöppelmeier et al., 2019).

As of yet, there is little handle on reconstructing the extent and intensity of past nepheloid layers and thus, how to assess the influence of past nepheloid layers on radionuclide scavenging. Based on analyzing changes in sediment focusing Gutjahr et al. (2008) suggested reduced focusing at BBOR intermediate depth sites indicating reduced shelf-derived sediment redistribution before the Holocene. Nepheloid layers are mostly produced by upper ocean dynamics of surface eddy kinetic energy propagating downwards stirring up bottom sediments (Gardner et al., 2018). During glacial periods the sea level was lower and the shelf contact area reduced. As a consequence energy from shallow tidal mixing on the shelves was nearly absent and the tidal energy increasingly dissipated in the deep ocean (Egbert et al., 2004; Wilmes et al., 2019). Bringing this tidal energy into the deep Atlantic would increase the mixing and turbulence there. As a consequence nepheloid layers during the LGM could have been greater and denser in the northwestern Atlantic. The greater suspended particle concentration could have increased the bottom scavenging of ^{231}Pa and ^{230}Th during the LGM (c.f. Deng et al., 2014; Hayes et al., 2015a).

Based on these observations and as anticipation of the discussion on differences in ^{231}Pa/^{230}Th between the BBOR and the Bermuda Rise we can deduce that nepheloid layers may not have had first order control on the down-core evolution of the new ^{231}Pa/^{230}Th records during the Holocene. Bottom scavenging by nepheloid layers was presumably more intense before the Holocene. Significantly and constantly higher ^{231}Pa/^{230}Th values at the BBOR in the glacial and deglacial parts could then be explained by the occurrence of nepheloid layers. However, assuming that the distribution of nepheloid layers during the LGM was similar to todays, it would be expected that bottom scavenging at the Bermuda Rise was more intense than at the BBOR. During the LGM lower ^{231}Pa/^{230}Th values at the Bermuda Rise are observed compared to the BBOR rendering a primary control of bottom scavenging on the ^{231}Pa/^{230}Th as unlikely. Since our knowledge about the distribution and size of nepheloid layers during the LGM is limited and relies on assumptions only, we cannot clearly exclude the effect of nepheloid layers on ^{231}Pa/^{230}Th, but suggest that it was not

dominant based on above observations. Moreover, increased bottom scavenging by nepheloid layers during the LGM is also pending to be confirmed.

4.2. Stable Holocene circulation

Today, the northwestern Atlantic basin is dominated by the southward export of NADW as main part of the AMOC. In contrast to this, in the northeastern Atlantic NADW flows partly northward as it enters the basin as far south as the equator (Rhein et al., 2015). Concentrations of dissolved ^{230}Th and ^{231}Pa in the eastern part of the North Atlantic show a depth dependent increase as a result of weaker export (Hayes et al. 2015a). In contrast, the western basin exhibits a moderate increase in dissolved ^{231}Pa concentrations with water depth due to the southward advection of ^{231}Pa by the strong overturning circulation (Deng et al., 2018). We therefore aim for considering ^{231}Pa/^{230}Th based AMOC reconstructions from regionally constrained data of the northwestern Atlantic (Ng et al., 2018; Lippold et al., 2011; Lippold et al., 2012b) instead of integrating ^{231}Pa/^{230}Th data from across the Atlantic (Yu et al., 1996; Lippold et al., 2016; Lippold et al., 2012a; Bradtmiller et al., 2014).

The notion of an active and strong Holocene AMOC (Keigwin and Boyle, 2000; Oppo et al., 2003) as indicated by low and relatively constant ^{231}Pa/^{230}Th at the Bermuda Rise is supported by low Holocene ^{231}Pa/^{230}Th values at the BBOR (average = 0.056 ± 3.2 %; Fig. 3). The strong overturning circulation is in accordance with strong NADW production as indicated by εNd indicating the prevalence of NSW in the northwestern Atlantic (Pöppelmeier et al., 2019). The absolute values of around 0.056 are well in agreement with previous ^{231}Pa/^{230}Th data compilations (Bradtmiller et al., 2014; Lippold et al., 2012a) for deep sites. An early Holocene AMOC strength overshoot as suggested by combined ^{231}Pa/^{230}Th and εNd records of lower time resolution (Lippold et al., 2016) cannot be confirmed from the new dataset.

4.3. Weaker circulation during the Last Glacial Maximum

All new down-core profiles display ^{231}Pa/^{230}Th values clearly higher during the LGM than during the Holocene (Figs. 4, 5), but on different absolute levels depending on the water depth. The shallowest Site 1059 (2984 m) features the overall lowest LGM values of all BBOR records. Following the finding that sedimentary ^{231}Pa/^{230}Th is largely a signal integrated from the 1000 m water column above the sea floor (Thomas et al., 2006, Luo et al., 2010), it seems likely that Site 1059 at least partially recorded the influence from a shallow

Glacial North Atlantic Intermediate Water (GNAIW) overturning cell above the core location. The existence of such a shallow overturning cell has been suggested by several nutrient-proxy based studies (e.g. Boyle and Keigwin, 1987; Duplessey et al., 1988; Oppo and Lehmann, 1993; Keigwin et al., 2004; Curry and Oppo, 2005) as well as observations from sortable silt data from the BBOR (Evans and Hall, 2008). Highest LGM values are found at the depth interval from 3500 to 4000 m (Site 1060/1061; Fig. 4a) suggesting either the influence of bottom scavenging or weaker water transport at these depths. The interpretation of a weaker water transport seems more plausible since the effect of bottom scavenging at the BBOR is subordinate to the large scale Pa export from the North to the South Atlantic (c.f. section 4.1.). A slight decrease in $^{231}Pa/^{230}Th$ during the LGM is observed in the cores below 4000 m (12JPC and Site 1062), indicative of a more active circulation in the abyssal northwestern Atlantic (Figs. 2, 3). Such a circulation depth-structure has also been reported from BBOR sortable silt reconstructions (Evans and Hall, 2008). Stable carbon isotope data ($\delta^{13}C$) from a depth transect along the BBOR show lighter $\delta^{13}C$ values with increasing water depth interpreted as propagating SSW during the LGM (Keigwin, 2004; Evans and Hall, 2008). However, in the light of recent findings of past water mass distributions in the western Atlantic basin from a $\delta^{13}C$ and Nd isotope perspective an extensive advance of SSW into the North Atlantic may need to be seen more critically (Gebbie 2014; Howe et al., 2016; Oppo et al., 2018; Spooner et al., 2018).

The study by Spooner et al. (2018) gives an estimation on the depth where the boundary between GNAIW and SSW was located at 30°S in the South Atlantic. Their data support a strong southward directed circulation at least in depths shallower than 2600 m. Furthermore, they found faster flow speeds below ~4000 m water depth interpreted as northward propagated SSW. Spooner et al. (2018) therefore suggested that the boundary between GNAIW and SSW at 30°S was situated somewhere between 2600 and ~4000 m water depth possibly in deeper than in shallow depths. This boundary is rather expected to descend towards 30°N instead of being stable on such a long distance due to the increasing dominance of NSW with shorter distance to the North Atlantic deep water formation areas (Gebbie 2014; Howe et al., 2016; Oppo et al., 2018). Accordingly, a strong inflow of SSW in the deep northwestern Atlantic basin during the LGM appears unlikely. A more recent study based on Nd isotopes argues that the northwestern Atlantic was filled mainly with NSW rather than SSW during the LGM (Howe et al., 2016), which is supported by proxy-model comparisons concluding that the volume seized by NSW was not much different in the LGM than in the

Holocene (Gebbie, 2014). The clearly more radiogenic Nd isotopic signatures before the Deglacial is not necessarily an unequivocal evidence for the presence of SSW as interpreted in earlier studies (Lippold et al., 2016; Gutjahr et al., 2008; Roberts et al., 2010), since the εNd end-members for both SSW and NSW potentially have changed towards more radiogenic values (Gutjahr et al., 2008; Skinner et al., 2013; Howe et al., 2016). From these findings it is difficult to maintain the notion of SSW predominantly bathing the BBOR and the Bermuda Rise during the LGM. Analyses from all these sites provide very similar Nd isotope signatures indicating that the complete depth transect at the BBOR was bathed in the same water mass during the LGM (Gutjahr et al., 2008; Pöppelmeier et al., 2019, Roberts et al., 2010; Gutjahr and Lippold, 2011). In contrast to the uniform picture in Nd isotope signatures, $^{231}Pa/^{230}Th$ ratios at the Bermuda Rise (~4500 m water depth; McManus et al., 2004; Lippold et al., 2009) were significantly lower than at the BBOR during the LGM nearly reaching Holocene levels (Figs. 3, 4a; note the different color at ~4500 m between ~20 and ~24 ka compared to the predominant color of the water column above and below in Fig. 3).

New glacial water mass reconstructions from the northwestern Atlantic do not only argue for a shallow GNAIW overturning cell but also for an abyssal northern water mass, that potentially was formed by brine rejection (Howe et al., 2016; Keigwin and Swift, 2017; Pöppelmeier et al., 2018). Such an abyssal southward directed water mass advection could explain the low $^{231}Pa/^{230}Th$ observed at the Bermuda Rise, which might be corroborated by slightly lower peak LGM $^{231}Pa/^{230}Th$ values at the deepest BBOR Site 1062 compared to Sites 1060/1061 (Fig. 4a).

Accordingly, when considering the depth structure of $^{231}Pa/^{230}Th$ (Fig. 3), our new records are in line with the hypothesis of the northwestern Atlantic basin predominantly bathed by NSW rather than SSW during the LGM as inferred from Nd isotope records (Howe et al., 2016; Pöppelmeier et al., 2019).

4.4. Confirming deglacial AMOC variability

The $^{231}Pa/^{230}Th$ record of Site 12JPC (4250 m) differs from the most proximal cores in the depth transect, namely Site 1061 (4036 m) and Site 1062 (4760 m) during the deglaciation (11 to 19 ka). While the latter records display deglacial millennial scale features, these are missing in the 12JPC record exhibiting a small plateau during the B/A only. Similarly, the Nd

isotope record of 12JPC also shows only a gradual glacial-interglacial shift (Pöppelmeier et al., 2019). Sedimentary depositional processes (e.g. winnowing or sediment redistribution; Gutjahr et al., 2008; Pöppelmeier et al., 2019) may have played a role in smoothing out the original oceanographic signal at this site. Sediment focusing during the YD is smaller at 12JPC compared with Sites 1061 and 1062 (Fig. S5). On this basis, we exclude the deglacial part of 12JPC from the following discussion as was done by Pöppelmeier et al. (2019).

Substantial freshwater input into the North Atlantic has been associated with a reduced (Bradtmiller et al., 2014) or almost collapsed (McManus et al., 2004) AMOC during HS1. Our results confirm a homogeneously reduced deep circulation regime during HS1 for all considered water depths, with average $^{231}Pa/^{230}Th$ of 0.081 (Figs. 2, 3; below 0.093), pointing to a widely weakened but still active overturning (Bradtmiller et al., 2014). Increases in $^{231}Pa/^{230}Th$ from LGM to HS1 are less pronounced for the water depth interval from 3500 to 4200 m (Sites 1060, 1061 and 12JPC; Figs. 3, 5) featuring the highest LGM values of the northwestern Atlantic depth transect and thus calling for a weaker change in circulation strength between LGM and HS1. In contrast, the deepest Site 1062 features a more pronounced increase in $^{231}Pa/^{230}Th$ from the LGM to HS1, potentially due to an abyssal component of northern sourced glacial water mass during the LGM (Howe et al., 2016; Keigwin and Swift, 2017; Pöppelmeier et al., 2018). Accordingly, increases in $^{231}Pa/^{230}Th$ from the LGM to HS1 below 4200 m indicate a weakening of glacial abyssal NSW water mass admixture. Thus, the new dataset further strengthens the notion of a sluggish AMOC during HS1 in the northwestern Atlantic for a wide range of water depths (Lund et al. 2015; Robinson et al., 2005; Bradtmiller et al., 2014; Fig. 3).

Following HS1, the onset of the B/A warm period is marked by an abrupt decrease in $^{231}Pa/^{230}Th$ in the BBOR cores reflecting the invigoration of the AMOC very similar to the Bermuda Rise record (McManus et al., 2004; Fig. 3). It has been proposed that the B/A was potentially marked not only by an AMOC reinvigoration but by an AMOC overshoot transiently producing more NADW than during the Holocene (e.g. Barker et al., 2010; Cheng et al., 2014). Such a B/A-overshoot is not apparent from the new records, even if taken into account that there is a certain response time of sedimentary $^{231}Pa/^{230}Th$ to AMOC changes as well as a potential smoothing of the signal by bioturbation. If such a B/A-overshoot was shorter than 200-500 years it may not have been fully recorded in its whole character in the sediment due to an interplay of sedimentation rate and processes like bioturbation smearing

sedimentary signals (Rempfer et al., 2017; Yu et al., 1996; Marchal et al., 2000). However, the high sedimentation rates at the BBOR (10-40 cm/ka) and in particular the duration of the B/A (~2ka) are expected to allow any $^{231}Pa/^{230}Th$ minima to be fully resolved. Thus, our new data from the BBOR (Fig. 2, 3) confirm the relatively abrupt onset of deep circulation but do not favor an extraordinarily strong long-lived AMOC strength overshoot during the B/A.

For all cores, low $^{231}Pa/^{230}Th$ during the B/A are terminated by a sharp increase towards almost LGM-like values during the YD for the whole depth transect (Fig. 3). During this last cold spell preceding the Holocene, the water mass distribution and circulation regime in the northwestern Atlantic basin below 3000 m water depth was again similar to these during the LGM and HS1 (Pöppelmeier et al., 2019). During the YD $^{231}Pa/^{230}Th$ averages to around 0.073 for all investigated water depths and thus indicates a weakened circulation but not as weak as the situation during HS1. After the YD all records evolved steadily towards low $^{231}Pa/^{230}Th$ values reflecting a prolonged and continuous establishment of the deep Holocene AMOC.

4.5. Heinrich Stadial 2

At the BBOR, the highest $^{231}Pa/^{230}Th$ values are observed during HS2 (Figs. 2, 3). In addition, this time period is characterized by a remarkably high variability in $^{231}Pa/^{230}Th$. These features are less pronounced at the shallowest Site 1059 which records $^{231}Pa/^{230}Th$ values similar to the LGM. The deeper cores with characteristic peaks and relatively high inner-HS2 variability are reminiscent of the record from the Bermuda Rise (Site 1063; Lippold et al., 2009). At the Bermuda Rise, AMOC reductions along with high diatom counts have been made responsible for high HS2 $^{231}Pa/^{230}Th$ (Lippold et al., 2009). However, even during peaks of high diatom abundances the absolute opal bulk concentrations of the sediments do not exceed 6 % (Böhm et al., 2015). Since Bermuda Rise and BBOR cores feature very high sedimentation rates a fairly good preservation of opal can be expected leading to the assumption that the buried opal is representative of the past opal flux. On a basin wide scale there is no significant correlation of opal concentration with $^{231}Pa/^{230}Th$ (Bradtmiller et al., 2014; Lippold et al., 2012a) for opal concentrations below 10 %. For all BBOR cores opal contents are very low (< 4 %; c.f. section 3.2.) and opal fluxes are thus unlikely to be a predominant factor controlling $^{231}Pa/^{230}Th$ for this region. Since the biogenic opal flux is an unlikely main factor controlling $^{231}Pa/^{230}Th$ during Heinrich Stadials the density distribution (Fig. 4b) from Sites 1060/1061 and the Bermuda Rise was on average not very different between HS2 and HS1 in terms of absolute $^{231}Pa/^{230}Th$ values. We suggest that both might have been similar in terms of circulation strength as well.

4.6. Comparison to $^{231}Pa/^{230}Th$ records from the equatorial Atlantic

For a more comprehensive investigation of glacial/interglacial changes of the West Atlantic DWBC we compare available $^{231}Pa/^{230}Th$ down-core profiles from the north and equatorial western Atlantic to our new dataset. This comprises four $^{231}Pa/^{230}Th$ records from the Ceara Rise (GeoB1515-1; GeoB1523-1; EW9209 1JPC; EW9209 3JPC; Lippold et al., 2016; Ng et al., 2018) and one from slightly north of the equator (RC 16-66; Bradtmiller et al., 2007) spanning water depths from 3100 to 4400 m (Fig. 1; Fig. S6; see section 2.4.). The $^{231}Pa/^{230}Th$ records of GeoB1515-1 and GeoB1523-1 have been improved by additional $^{231}Pa/^{230}Th$ data and age control points shifting the highest values of the records ~2 ka towards older ages (Lippold et al., 2016) in line with the timing of HS1 (Table S6). Most of these records exhibit clearly lower time resolution than the new BBOR records. For this reason, we only compare the time-slices of the Holocene, LGM and HS1 with our findings

(Fig. 5). The equatorial records show the common feature of low Holocene $^{231}Pa/^{230}Th$ and higher deglacial and glacial $^{231}Pa/^{230}Th$ levels and a more or less well resolved peak around HS1. These characteristics are in good agreement with the new higher resolution BBOR records calling for a large-scale oceanographic feature on this time-scale for this range of water depths. While the absolute $^{231}Pa/^{230}Th$ values of the shallower cores (GeoB1515-1; GeoB1523-1; EW9209 3JPC; 3100 to 3300 m) are in good agreement to the new BBOR records, $^{231}Pa/^{230}Th$ values from the deeper equatorial sites (EW9209 1JPC; RC 16-66; 4000 to 4500 m) are considerably lower (Fig. 5). One would expect the $^{231}Pa/^{230}Th$ ratio to increase with a longer traveling time of NADW (greater distance to the deep water formation zone). While ^{230}Th is quickly scavenged from the water column advected ^{231}Pa can be supplied to sites further south from upstream (north) and the concentration is further increased by the continuous ingrowth from the decay of dissolved ^{235}U. However, the relationship between water mass aging and increasing $^{231}Pa/^{230}Th$ is still unclear (Deng et al., 2018). Lower $^{231}Pa/^{230}Th$ at greater depth further downstream of NADW (equatorial Atlantic) can rather be explained by the effect of building up a ^{231}Pa deficit relative to ^{230}Th within one individual overturning cell (Burckel et al., 2016; Luo et al., 2010). Alternatively, the lower equatorial $^{231}Pa/^{230}Th$ values observed may also reflect the effect of bathymetry and the narrowing of the DWBC flow path in the region, leading to increased flow speeds at greater depths. Taken together, all sites from below ~3000 m water depth and within the area influenced by the DWBC, display very similar patterns in the $^{231}Pa/^{230}Th$ down-core profiles confirming the general notion of the relative AMOC strengths being most vigorous during the Holocene and clearly weaker during the LGM with the weakest overturning during HS1.

5. Conclusions

We present four new high-resolution $^{231}Pa/^{230}Th$ records from the deep northwestern Atlantic covering the time period from Heinrich Stadial 2 until today, and resolve AMOC variability during climatic key intervals like the HS2, LGM, HS1, B/A, YD, and the Holocene. These new time-series confirm the timing and magnitude of the millennial scale climate variability previously established by the Bermuda Rise $^{231}Pa/^{230}Th$ records (such as gradual AMOC increase from the YD into the Holocene, no B/A AMOC overshoot, similar levels of HS1 and HS2 values but with higher variability of the latter) but with one exception. Whereas a strong LGM circulation was suggested by the Bermuda Rise record, the depth transect presented here shows a more complex circulation pattern. The BBOR records from 3500 to 4700 m suggest significantly reduced circulation strength during most of the LGM. In the water depth

from 3500 to 4000 m LGM $^{231}Pa/^{230}Th$ values are nearly indistinguishable from Heinrich Stadial 1 when the AMOC was weakened across the entire Atlantic. The shallowest location of our depth transect, Site 1059 at 3000 m water depth, again features lower $^{231}Pa/^{230}Th$ values during the LGM on a level similar to the Bermuda Rise in accordance with a shallow GNAIW overturning cell above. Further, comparison to existing equatorial West Atlantic $^{231}Pa/^{230}Th$ records yield a uniform basin-wide picture confirming a strong Holocene circulation regime, a weaker LGM overturning configuration and a mostly reduced circulation during Heinrich Stadial 1 and 2.

Acknowledgments

Stefan Rheinberger is thanked for technical support during ICP-MS measurements. Further, we acknowledge Sönke Szidat for the new ^{14}C date for GeoB1515-1 and Benny Antz for preliminary work on the ODP cores. We thank the IODP core repository in Bremen for providing the samples.

The comments of two anonymous reviewers considerably improved the manuscript. This study has been funded by the Emmy-Noether-Programme of the German Research Foundation (DFG) Grant Li1815/4. Data can be found in the supporting information and on Pangaea (https://doi.pangaea.de/10.1594/PANGAEA.908156).

References

Anderson, R. F., Bacon, M. P., Brewer, P. G., 1983. Removal of 230Th and 231Pa at ocean margins. Earth and Planetary Science Letters, 66(C), 73–90. doi:10.1016/0012-821X(83)90127-9

Anderson, R. F., Ali, S., Bradtmiller, L. I., Nielsen, S. H. H., Fleisher, M. Q., Anderson, B. E., Burckle, L. H., 2009. Wind-Driven Upwelling in the Southern Ocean and the Deglacial Rise in Atmospheric CO2. Science, 323, 1443–1448. doi:10.1126/science.1167441

Barker, S., Knorr, G., Vautravers, M. J., Diz, P., Skinner, L.C., 2010. Extreme deepening of the Atlantic overturning circulation during deglaciation. Nature Geoscience 3, 567–571. doi:10.1038/ngeo921

Blaser, P., Lippold, J., Gutjahr, M., Frank, N., Link, J. M., Frank, M., 2016. Extracting foraminiferal seawater Nd isotope signatures from bulk deep sea sediment by chemical leaching. Chemical Geology, 439, 189–204. doi:10.1016/j.chemgeo.2016.06.024

Böhm, E., Lippold, J., Gutjahr, M., Frank, M., Blaser, P., Antz, B., et al. 2015. Strong and deep Atlantic meridional overturning circulation during the last glacial cycle. Nature, 517(7532), 73–76. doi: 10.1038/nature14059

Boyle, E. A., & Keigwin, L., 1987. North-Atlantic Thermohaline Circulation during the Past 20,000 Years Linked to High-Latitude Surface-Temperature. Nature, 330, 35–40. doi: 10.1038/330035a0

Bradtmiller, L. I., Anderson, R. F., Fleisher, M. Q., Burckle, L.H., 2007. Opal burial in the equatorial Atlantic Ocean over the last 30 ka: Implications for glacial-interglacial changes in the ocean silicon cycle. Paleoceanography, 22, 1–15. doi:10.1029/2007PA001443

Bradtmiller, L. I., McManus, J. F., Robinson, L. F., 2014. 231Pa/230Th evidence for a weakened but persistent Atlantic meridional overturning circulation during Heinrich Stadial 1. Nature Communications, 5, 5817. doi:10.1038/ncomms6817

Broecker, W. S., Takahashi, T., & Takahashi, T., 1985. Sources and flow patterns of Deep-Ocean waters as deduced from potential temperature, salinity, and initial phosphate concentration. Journal of Geophysical Research, 90, 6925–6939. doi:10.1029/JC090iC04p06925

Burckel, P., Waelbroeck, C., Luo, Y., Roche, D. M., Pichat, S., Jaccard, S. L., Gherardi, J., Govin, A., Lippold, J., Thil, F., 2016. Changes in the geometry and strength of the Atlantic meridional overturning circulation during the last glacial (20-50 ka). Climate of the Past, 12, 2061–2075. doi:10.5194/cp-12-2061-2016

Chase, Z., Anderson, R. F., Fleisher, M. Q., Kubik, P. W., 2003. Scavenging of 230Th, 231Pa and 10Be in the Southern Ocean (SW Pacific sector): The importance of particle flux, particle composition and advection. Deep-Sea Research Part II, 50, 739–768. doi:10.1016/S0967-0645(02)00593-3

Chase, Z., Anderson, R. F., Fleisher, M. Q., Kubik, P. W., 2002. The influence of particle composition and particle flux on scavenging of Th, Pa and Be in the ocean. Earth and Planetary Science Letters, 204, 215–229. doi:10.1016/S0012-821X(02)00984-6

Cheng, J., Liu, Z., He, F., Otto-Bliesner, B., Brady, E., Lynch-Stieglitz, J., 2014. Model–proxy comparison for overshoot phenomenon of Atlantic thermohaline circulation at Bølling–Allerød. Chinese Science Bulletin, 59, 4510–4515. doi:10.1007/s11434-014-0586-x

Christl, M., Lippold, J., Hofmann, A., Wacker, L., Lahaye, Y., & Synal, H. A., 2010. 231Pa/230Th: A proxy for upwelling off the coast of West Africa. Nuclear Instruments and Methods in Physics Research, Section B: Beam Interactions with Materials and Atoms, 268(7–8), 1159–1162. doi:10.1016/j.nimb.2009.10.123

Costa, M. C., Jacobel, A. W., McManus, J. F., Anderson, R. F., Winckler, G., Thiagarajan, N., 2017. Productivity patterns in the equatorial Pacific over the last 30,000 years. Global Biogeochemical Cycles, 31(5), 850–865. doi:10.1002/2016gb005579

Curry, W. B., Oppo, D. W., 2005. Glacial water mass geometry and the distribution of δ 13C of ΣCO2 in the western Atlantic Ocean. Paleoceanography, 20, 1–12. doi:10.1029/2004PA001021

Deng, F., Thomas, A. L., Rijkenberg, M. J. A., & Henderson, G. M., 2014. Controls on seawater 231Pa, 230Th and 232Th concentrations along the flow paths of deep waters in the Southwest Atlantic. Earth and Planetary Science Letters, 390, 93–102. doi:10.1016/j.epsl.2013.12.038

Deng, F., Henderson, G. M., Castrillejo, M., Perez, F. F., 2018. Evolution of 231 Pa and 230 Th in overflow waters of the North Atlantic. Biogeosciences, 15, 7299-7313. doi:10.5194/bg-2018-191

Duplessy, J. C., Shackleton, N. J., Fairbanks, R. G., Labeyrie, L., Oppo, D., & Kallel, N., 1988. Deepwater source variations during the last climatic cycle and their impact on the global deepwater circulation. Paleoceanography, 3(3), 343–360. doi:10.1029/PA003i003p00343

Egbert, G. D., Ray, R. D., & Bills, B. G. (2004). Numerical modeling of the global semidiurnal tide in the present day and in the last glacial maximum. Journal of Geophysical Research C: Oceans, 109(3), 1–15. doi:10.1029/2003jc001973

Evans, H. K., Hall, I. R., 2008. Deepwater circulation on Blake Outer Ridge (western North Atlantic) during the Holocene, Younger Dryas, and Last Glacial Maximum. Geochemistry, Geophysics, Geosystems, 9, 1–19. doi:10.1029/2007GC001771

Fietzke, J., Bollhöfer, A., Frank, M., Mangini, A., 1999. Protactinium determination in manganese crust VA13/2 by thermal ionization mass spectrometry (TIMS). Nuclear Instruments and Methods in Physics Research, 149, 353–360. doi:10.1016/S0168-583X(98)00912-4

Garcia, H. E., Locarnini, R. A., Boyer, T. P., Antonov, J. I., Baranova, O. K., Zweng, M. M., Reagan, J. R., Johnson, D. R., 2014. World Ocean Atlas 2013, Volume 4: Dissolved Inorganic Nutrients (phosphate, nitrate, silicate). S. Levitus, Ed., A. Mishonov Technical Ed.; NOAA Atlas NESDIS 76, 25 pp.

Gardner, W. D., Richardson, M. J., Mishonov, A. V., 2018. Global assessment of benthic nepheloid layers and linkage with upper ocean dynamics. Earth and Planetary Science Letters, 482, 126–134. doi:10.1016/j.epsl.2017.11.008

Gebbie, G., 2014. How much did Glacial North Atlantic Water shoal?. Paleoceanography, 29, 190–209. doi:10.1002/2013PA002557

Geibert, W., Usbeck, R., 2004. Adsorption of thorium and protactinium onto different particle types: Experimental findings. Geochimica et Cosmochimica Acta, 68, 1489–1501. doi:10.1016/j.gca.2003.10.011

Gherardi, J. M., Labeyrie, L., Nave, S., Francois, R., McManus, J. F., Cortijo, E., 2009. Glacial-interglacial circulation changes inferred from 231Pa/230Th sedimentary record in the North Atlantic region. Paleoceanography, 24, 1–14. doi:10.1029/2008PA001696

Gottschalk, J., Szidat, S., Michel, E., Mazaud, A., Salazar, G., Battaglia, M., Lippold, J., Jaccard, S.L., 2018. Radiocarbon measurements of small-size foraminiferal samples with the mini carbon dating system (MICADAS) at the University of Bern: Implications for paleoclimate reconstructions. Radiocarbon, 60, 469–491. doi:10.1017/RDC.2018.3

Grützner, J., Giosan, L., Franz, S.O., Tiedemann, R., Cortijo, E., Chaisson, W. P., Flood, R. D., Hagen, S., Keigwin, L. D., Poli, S., Rio, D., Williams, T., 2002. Astronomical age models for Pleistocene drift sediments from the western North Atlantic (ODP sites 1055-1063). Marine Geology, 189, 5–23. doi:10.1016/S0025-3227(02)00320-1

Gutjahr, M., Frank, M., Stirling, C. H., Keigwin, L. D., Halliday, A. N., 2008. Tracing the Nd isotope evolution of North Atlantic Deep and Intermediate Waters in the western

North Atlantic since the Last Glacial Maximum from Blake Ridge sediments. Earth and Planetary Science Letters, 266, 61–77. doi:10.1016/j.epsl.2007.10.037

Gutjahr, M., Lippold, J., 2011. Early arrival of Southern Source Water in the deep North Atlantic prior to Heinrich event 2. Paleoceanography, 26, 1–9. doi:10.1029/2011PA002114

Hagen, S., Keigwin, L. D., 2002. Sea-surface temperature variability and deep water reorganisation in the subtropical North Atlantic during isotope stage 2-4. Marine Geology, 189, 145–162. doi:10.1016/S0025-3227(02)00327-4

Hayes, C. T., Anderson, R. F., Jaccard, S. L., François, R., Fleisher, M. Q., Soon, M., Gersonde, R., 2013. A new perspective on boundary scavenging in the North Pacific Ocean. Earth and Planetary Science Letters, 369–370, 86–97. doi:10.1016/j.epsl.2013.03.008

Hayes, C. T., Anderson, R. F., Fleisher, M. Q., Huang, K. F., Robinson, L. F., Lu, Y., Cheng, H., Edwards, R. L., Moran, S. B., 2015a. 230Th and 231Pa on GEOTRACES GA03, the U.S. GEOTRACES North Atlantic transect, and implications for modern and paleoceanographic chemical fluxes. Deep-Sea Research, 116, 29–41. doi:10.1016/j.dsr2.2014.07.007

Hayes, C. T., Anderson, R. F., Fleisher, M. Q., Vivancos, S. M., Lam, P. J., Ohnemus, D. C., et al., 2015b. Intensity of Th and Pa scavenging partitioned by particle chemistry in the North Atlantic Ocean. Marine Chemistry, 170, 49–60. doi:10.1016/j.marchem.2015.01.006

Henderson, G. M., Anderson, R. F., 2003. The U-series Toolbox for Paleoceanography. Reviews in mineralogy and geochemistry, 52, 493–531. doi:10.2113/0520493

Hoffmann, S. S., 2018. Evidence for Stable Holocene Basin-Scale Overturning Circulation Despite Variable Currents Along the Deep Western Boundary of the North Atlantic Ocean. Geophysical Research Letters, 45, 13427-13436. doi:10.1029/2018GL080187

Howe, J. N. W., Piotrowski, A. M., Noble, T. L., Mulitza, S., Chiessi, C.M., Bayon, G., 2016. North Atlantic Deep Water Production during the Last Glacial Maximum. Nature Communications, 7, 1–8. doi:10.1038/ncomms11765

Howe, J. N. W., Piotrowski, A. M., Hu, R., & Bory, A. (2017). Reconstruction of east – west deep water exchange in the low latitude Atlantic Ocean over the past 25,000 years. Earth and Planetary Science Letters, 458, 327–336. doi:10.1016/j.epsl.2016.10.048

Johnson, G. C., 2008. Quantifying Antarctic Bottom Water and North Atlantic Deep Water volumes. Journal of Geophysical Research, 113, 1–13. doi:10.1029/2007JC004477

Keigwin, L. D., & Boyle, E. A., 2000. Detecting Holocene changes in thermohaline circulation. Proceedings of the National Academy of Sciences, 97(4), 1343–1346. doi:10.1073/pnas.97.4.1343

Keigwin, L. D., & Schlegel, M., (2002). Ocean ventilation and sedimentation since the glacial maximum at 3 km in the western North Atlantic. Geochemistry, Geophysics, Geosystems 3 (6). doi:10.1029/2001GC000283

Keigwin, L. D., 2004. Radiocarbon and stable isotope constraints on Last Glacial Maximum and Younger Dryas ventilation in the western North Atlantic. Paleoceanography, 19, 1–15. doi:10.1029/2004PA001029

Keigwin, L. D., Jones, G.A., 1994. Western North Atlantic evidence for millennial-scale changes in ocean circulation and climate. Journal of Geophysical Research, 99, 12397-12410. doi:10.1029/94JC00525

Keigwin, L. D., Swift, S.A., 2017. Carbon isotope evidence for a northern source of deep water in the glacial western North Atlantic. Proceedings of the National Academy of Science, 114, 2831–2835. doi:10.1073/pnas.1614693114

Korff, L., von Dobeneck, T., Frederichs, T., Kasten, S., Kuhn, G., Gersonde, R., & Diekmann, B. (2016). Cyclic magnetite dissolution in Pleistocene sediments of the abyssal northwest Pacific Ocean: Evidence for glacial oxygen depletion and carbon trapping. Paleoceanography, 31(5), 600–624. doi:10.1002/2015PA002882

Lippold, J., Grützner, J., Winter, D., Lahaye, Y., Mangini, A., Christi, M., 2009. Does sedimentary 231Pa/230Th from the Bermuda Rise monitor past Atlantic Meridional Overturning Circulation? Geophysical Research Letters, 36, 1–6. doi:10.1029/2009GL038068

Lippold, J., Gutjahr, M., Blaser, P., Christner, E., de Carvalho Ferreira, M. L., Mulitza, S., Christl, M., Wombacher, F., Böhm, E., Antz, B., Cartapanis, O., Vogel, H., Jaccard, S.L., 2016. Deep water provenance and dynamics of the (de)glacial Atlantic meridional overturning circulation. Earth and Planetary Science Letters, 445, 68–78. doi:10.1016/j.epsl.2016.04.013

Lippold, J., Luo, Y., Francois, R., Allen, S.E., Gherardi, J., Pichat, S., Hickey, B., Schulz, H., 2012a. Strength and geometry of the glacial Atlantic Meridional Overturning Circulation. Nature Geoscience, 5, 813–816. doi:10.1038/ngeo1608

Lippold, J., Mulitza, S., Mollenhauer, G., Weyer, S., Heslop, D., Christl, M., 2012b. Boundary scavenging at the East Atlantic margin does not negate use of 231Pa/230Th to trace Atlantic overturning. Earth and Planetary Science Letters, 333–334, 317–331. doi:10.1016/j.epsl.2012.04.005

Lippold, J., Gherardi, J. M., Luo, Y., 2011. Testing the 231Pa/230Th paleocirculation proxy: A data versus 2D model comparison. Geophysical Research Letters, 38, 1–7. doi:10.1029/2011GL049282

Locarnini, R. A., Mishonov, A. V., Antonov, J. I., Boyer, T. P., Garcia, H. E., Baranova, O. K., Zweng, M. M., Paver, C. R., Reagan, J. R., Johnson, D. R., Hamilton, M., Seidov, D., 2013. World Ocean Atlas 2013, Volume 1: Temperature. S. Levitus, Ed., A. Mishonov Technical Ed.; NOAA Atlas NESDIS 73, 40 pp.

Lynch-Stieglitz, J., 2017. The Atlantic Meridional Overturning Circulation and Abrupt Climate Change. Annual Review of Marine Science, 9, 83–104. doi:10.1146/annurev-marine-010816-060415

Lynch-Stieglitz, J., Schmidt, M. W., Gene Henry, L., Curry, W. B., Skinner, L. C., Mulitza, S., Zhang, R., Chang, P., 2014. Muted change in Atlantic overturning circulation over some glacial-aged Heinrich events. Nature Geoscience, 7, 144–150. doi:10.1038/ngeo2045

Lund, D. C., Tessin, A. C., Hoffman, J. L., Schmittner, A., 2015. Southwest Atlantic water mass evolution during the last deglaciation. Paleoceanography, 30, 477–494. doi:10.1002/2014PA002657

Lund, D. C., Pavia, F. J., Seeley, E. I., McCart, S. E., Rafter, P. A., Farley, K. A., et al. (2019). Hydrothermal scavenging of 230Th on the Southern East Pacific Rise during

the last deglaciation. Earth and Planetary Science Letters, 510, 64–72. doi:10.1016/j.epsl.2018.12.037

Luo, Y., Francois, R., Allen, S., 2010. Sediment 231Pa/230Th as a recorder of the rate of the Atlantic meridional overturning circulation: insights from a 2-D model. Ocean Science, 6, 381–400. doi:10.5194/os-6-381-2010

Marchal, O., Francois, R., Stocker, T. F., Joos, F., 2000. Ocean thermohaline circulation and sedimentary 231Pa/230Th ratio. Paleoceanography, 15, 625–641. doi:10.1029/2000PA000496

Marchitto, T. M., Broecker, W. S., 2006. Deep water mass geometry in the glacial Atlantic Ocean: A review of constraints from the paleonutrient proxy Cd/Ca. Geochemistry Geophysics Geosystems, 7(12), 1525-2027. doi:10.1029/2006GC001323

McCave, I. N., Manighetti, B., Robinson, S.G., 1995. Sortable silt and fine sediment size/composition slicing: Parameters for palaeocurrent speed and palaeoceanography. Paleoceanography, 10(3), 593–610. Doi:10.1029/94PA03039

McCave, I. N., Thornalley, D. J. R., Hall, I. R., 2017. Relation of sortable silt grain-size to deep-sea current speeds: Calibration of the 'Mud Current Meter.' Deep-Sea Research Part I, 127, 1–12. doi:10.1016/j.dsr.2017.07.003

McManus, J. F., Francois, R., Gherardi, J.-M., Keigwin, L. D., Brown-Leger, S., 2004. Collapse and rapid resumption of Atlantic meridional circulation linked to deglacial climate changes. Nature, 428, 834–837. doi:10.1038/nature02494

Missiaen, L., Pichat, S., Waelbroeck, C., Douville, E., Bordier, L., Dapoigny, A., Thil, F., Foliot, L., Wacker, L., 2018. Downcore Variations of Sedimentary Detrital (238U/232Th) Ratio: Implications on the Use of230Thxsand231Paxsto Reconstruct Sediment Flux and Ocean Circulation. Geochemistry Geophysics Geosystems, 19, 2560–2573. doi:10.1029/2017GC007410

Müller, P. J., Schneider, R., 1993. An automated leaching method for the determination of opal in sediments and particulate matter. Deep-Sea Research Part I, 40, 425–444. doi:10.1016/0967-0637(93)90140-X

Ng, H. C., Robinson, L. F., McManus, J. F., Mohamed, K. J., Jacobel, A. W., Ivanovic, R. F., Gregoire, L. J., Chen, T., 2018. Coherent deglacial changes in western Atlantic Ocean circulation. Nature Communications, 9, 1–10. doi:10.1038/s41467-018-05312-3

Oppo, D. W., & Lehman, S. J., 1993. Mid-depth circulation of the subpolar North Atlantic during the last glacial maximum. Science, 259, 1148–1152. doi:10.1126/science.259.5098.1148

Oppo, D. W., McManus, J. F., & Cullen, J. L., 2003. Deepwater variability in the Holocene epoch. Nature, 422(6929), 277–277. doi:10.1038/422277b

Oppo, D. W., Gebbie, G., Huang, K.-F., Curry, W.B., Marchitto, T. M., Pietro, K. R., 2018. Data Constraints on Glacial Atlantic Water Mass Geometry and Properties. Paleoceanography and Paleoclimatology, 33(9), 1013-1034. doi:10.1029/2018PA003408

Pavia, F., Anderson, R., Vivancos, S., Fleisher, M., Lam, P., Lu, Y., Cheng, H., Zhang, P., Lawrence Edwards, R., 2018. Intense hydrothermal scavenging of 230Th and 231Pa in the deep Southeast Pacific. Marine Chemistry, 201, 212–228. doi:10.1016/j.marchem.2017.08.003

Piotrowski, A. M., Goldstein, S. L., Hemming, S. R., Fairbanks, R. G., 2005. Temporal relationships between ocean circulation and carbon cycling during glacial-interglacial transitions. Science, 307, 1933–1938. doi:10.1126/science.1104883

Pöppelmeier, F., Gutjahr, M., Blaser, P., Keigwin, L. D., Lippold, J., 2018. Origin of abyssal NW Atlantic water masses since the Last Glacial Maximum. Paleoceanography and Paleoclimatology, 17, 1–14. doi:10.1029/2017PA003290

Pöppelmeier, F., Blaser, P., Gutjahr, M., Süfke, F., Thornalley, D. J. R., Grützner, J., Jakob, K. A., Link, J. M., Szidat, S., Lippold, J., 2019. Influence of Ocean Circulation and Benthic Exchange on Deep Northwest Atlantic Nd Isotope Records During the Past 30,000 Years. Geochemistry, Geophysics, Geosystems, 20, 4457-4469, doi:10.1029/2019GC008271

Reimer, P. J., Bard, E., Bayliss, A., Beck, J. W., Blackwell, P. G., Ramsey, C. B., et al. (2013). IntCal13 and Marine13 radiocarbon age calibration curves 0-50,000 years cal BP. Radiocarbon, 55(4), 1869-1887. doi:10.2458/azu_js_rc.55.16947

Regelous, M., Turner, S. P., Elliott, T. R., Rostami, K., Hawkesworth, C. J., 2004. Measurement of femtogram quantities of protactinium in silicate rock samples by multicollector inductively coupled plasma mass spectrometry. Analytical Chemistry, 76, 3584–3589. doi:10.1021/ac030374l

Rempfer, J., Stocker, T. F., Joos, F., Lippold, J., Jaccard, S.L., 2017. New insights into cycling of 231Pa and 230Th in the Atlantic Ocean. Earth and Planetary Science Letters, 468, 27–37. doi:10.1016/j.epsl.2017.03.027

Rhein, M., Kieke, D., Steinfeldt, R., 2015. Advection of North Atlantic Deep Water from the Labrador Sea to the southern hemisphere. Journal of Geophyscal Research, 120, 2471–2487. doi:10.1002/2014JC010605

Roberts, N. L., Piotrowski, A. M., McManus, J. F., Keigwin, L. D., 2010. Synchronous deglacial overturning and water mass source changes. Science, 327, 75–78. doi:10.1126/science.1178068

Robinson, L. F., Adkins, J. F., Keigwin, L. D., Southon, J., Fernandez, D. P., Wang, S.-L., Scheirer, D. S., 2005. Radiocarbon Variability in the Western North Atlantic During the Last Deglaciation. Science, 310, 1469–1473. doi:10.1126/science.1114832

Rothwell, R. G., Croudace, I. W., 2015. Micro-XRF Studies of Sediment Cores, Developments in Paleoenvironmental Research, 17. doi:10.1007/978-94-017-9849-5_2

Rutgers van der Loeff, M., Venchiarutti, C., Stimac, I., Ooijen, J. Van, Huhn, O., Rohardt, G., Strass, V., 2016. Meridional circulation across the Antarctic Circumpolar Current serves as a double 231Pa and 230Th trap. Earth and Planetary Science Letters, 455, 73–84. doi:10.1016/j.epsl.2016.07.027

Scholten, J. C., Fietzke, J., Mangini, A., Garbe-Schönberg, C. D., Eisenhauer, A., Schneider, R., & Stoffers, P., 2008. Advection and scavenging: Effects on 230Th and 231Pa distribution off Southwest Africa. Earth and Planetary Science Letters, 271(1–4), 159–169. doi:10.1016/j.epsl.2008.03.060

Skinner, L. C., Scrivner, A. E., Vance, D., Barker, S., Fallon, S., & Waelbroeck, C. (2013). North atlantic versus southern ocean contributions to a deglacial surge in deep ocean ventilation. Geology, 41(6), 667–670. doi:10.1130/G34133.1

Spooner, P. T., Thornalley, D. J. R., Ellis, P., 2018. Grain Size Constraints on Glacial Circulation in the Southwest Atlantic. Paleoceanography and Paleoclimatology, 33, 21–30. doi:10.1002/2017PA003232

Stahr, F. R., & Sanford, T. B., 1999. Transport and bottom boundary layer observations of the North Atlantic Deep Western Boundary Current at the Blake Outer Ridge. Deep-Sea Research Part II: Topical Studies in Oceanography, 46(1–2), 205–243. doi:10.1016/S0967-0645(98)00101-5

Süfke, F., Lippold, J., Happel, S., 2018. Improved Separation of Pa from Th and U in Marine Sediments with TK400 Resin. Analytical Chemistry, 90, 1395–1401. doi:10.1021/acs.analchem.7b04723

Thomas, A. L., Henderson, G. M., Robinson, L. F., 2006. Interpretation of the 231Pa/230Th paleocirculation proxy: New water-column measurements from the southwest Indian Ocean. Earth and Planetary Science Letters, 241, 493–504. doi:10.1016/j.epsl.2005.11.031

Thornalley, D. J. R., Barker, S., Becker, J., Hall, I. R., Knorr, G., 2013. Abrupt changes in deep Atlantic circulation during the transition to full glacial conditions. Paleoceanography, 28, 253–262. doi:10.1002/palo.20025

Walter, H. J., Rutgers van der Loeff, M., Hoeltzen, H., 1997. Enhanced scavenging of 231Pa relative to 230Th in the South Atlantic south of the Polar Front: Implications for the use of the 231Pa/230Th ratio as a paleoproductivity proxy. Earth and Planetary Science Letters, 149, 85–100. doi:10.1016/S0012-821X(97)00068-X

Wilmes, S. -B., Schmittner, A., & Green, J. A. M. (2019). Glacial ice sheet extent effects on modeled tidal mixing and the global overturning circulation. Paleoceanography and Paleoclimatology, 2019PA003644. doi:10.1029/2019PA003644

Yu, E.-F., Francois, R., & Bacon, M. P. (1996). Similar rates of modern and last-glacial ocean thermohaline circulation inferred from radiochemical data. Nature, 379, 689-694. doi:10.1038/379689a0

Zweng, M. M., Reagan, J. R., Antonov, J. I., Locarnini, R.A., Mishonov, A. V., Boyer, T. P., Garcia, H. E., Baranova, O. K., Johnson, D. R., Seidov, D., Biddle, M. M., 2013. World Ocean Atlas 2013, Volume 2: Salinity. S. Levitus, Ed., A. Mishonov Technical Ed.; NOAA Atlas NESDIS 74, 39 pp.

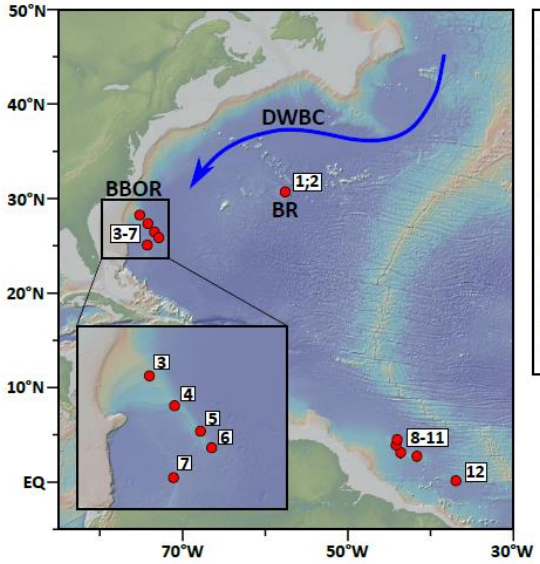

Site	Core	Latitude	Longitude	Depth (m)	References
1	OCE326-GGC5	33.70°N	57.58°W	4550	McManus et al. (2004)
2	ODP 1063	33.68°N	57.62°W	4584	Lippold et al. (2009)
3	ODP 1059	31.40°N	75.25°W	2984	this study
4	ODP 1060	30.45°N	74.28°W	3480	this study
5	ODP 1061	29.58°N	73.35°W	4036	this study
6	KNR140 12JPC	29.04°N	72.53°W	4250	Lippold et al. (2016); this study
7	ODP 1062	28.14°N	74.24°W	4760	this study
8	EW9209-1JPC	5.90°N	44.19°W	4056	Ng et al. (2018)
9	EW9209-3JPC	5.31°N	44.26°W	3288	Ng et al. (2018)
10	GeoB1515-1	4.24°N	43.67°W	3129	Lippold et al. (2016); this study
11	GeoB1523-1	3.83°N	41.62°W	3292	Lippold et al. (2016); this study
12	RC16-66	0.75°N	36.61°W	4424	Bradtmiller et al. (2007)

Figure 1: Overview map of the northwest Atlantic. Core locations presented/discussed in this study are indicated in red. The main study area is the northwestern Atlantic with the Blake-Bahama-Outer-Ridge (BBOR) and the Bermuda Rise (BR). The blue arrow depicts the Deep Western Boundary Current (DWBC) path from the northern North Atlantic along the North American margin (Thornalley et al., 2013). The table gives core parameters and references.

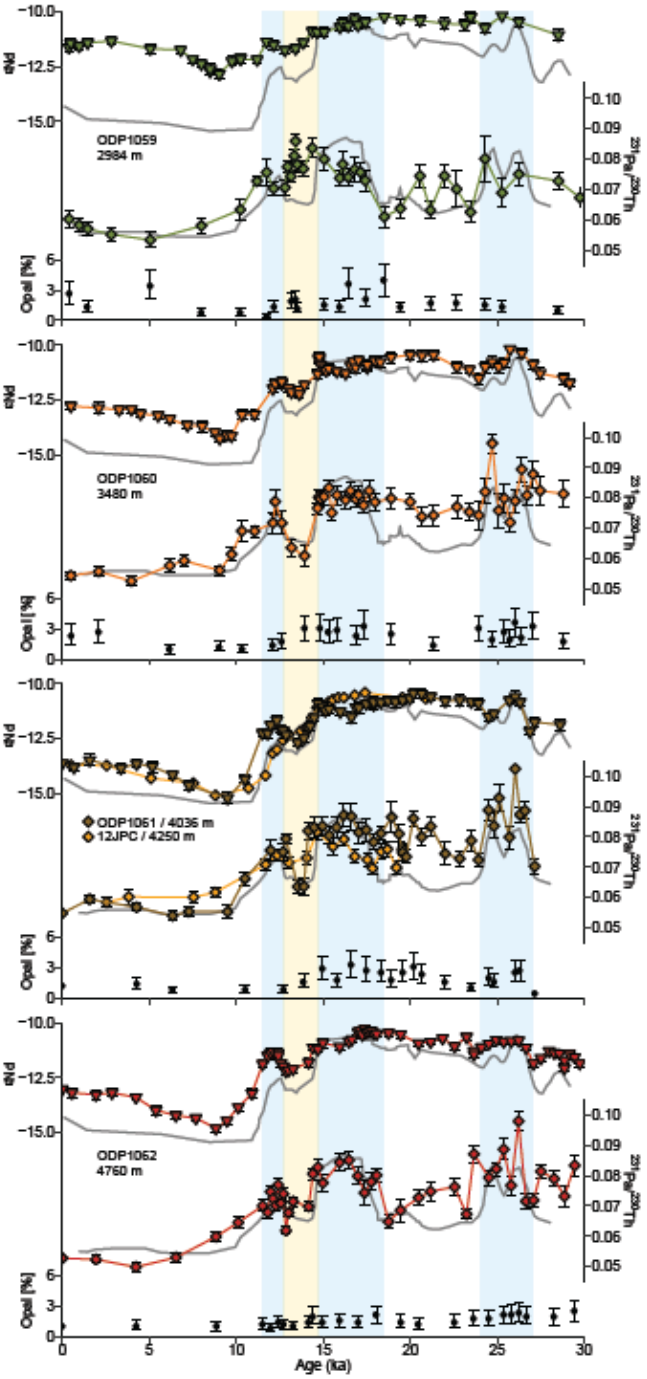

Figure 2: $^{231}Pa/^{230}Th$ (diamonds) and biogenic opal (black dots) records from this study complemented by Nd isotope records (downward triangles) denoted as εNd ($^{143}Nd/^{144}Nd$ normalized to the Chondritic Uniform Reservoir in parts per ten thousand) of the BBOR cores (Pöppelmeier et al., 2019). For all panels the gray background lines depict $^{231}Pa/^{230}Th$ and Nd isotope records from the Bermuda Rise for comparison (McManus et al., 2004; Lippold et al., 2009; Roberts et al., 2010; Gutjahr and Lippold, 2011). The blue vertical bars indicate the cold periods YD, HS1 and HS2, respectively. The yellow vertical bar marks the B/A warm period.

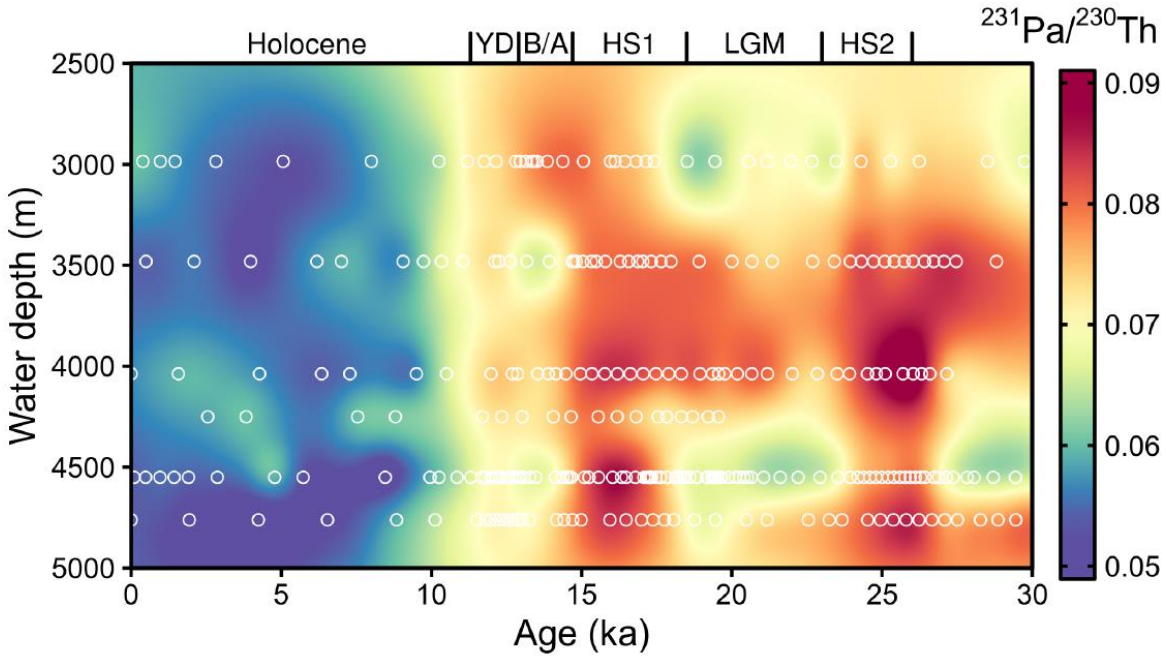

Figure 3: Hovmøller diagram of the BBOR and Bermuda Rise $^{231}Pa/^{230}Th$ reconstructions covering the last 30 ka (data from McManus et al., 2004, Lippold et al., 2009 and this study). White circles indicate data points.

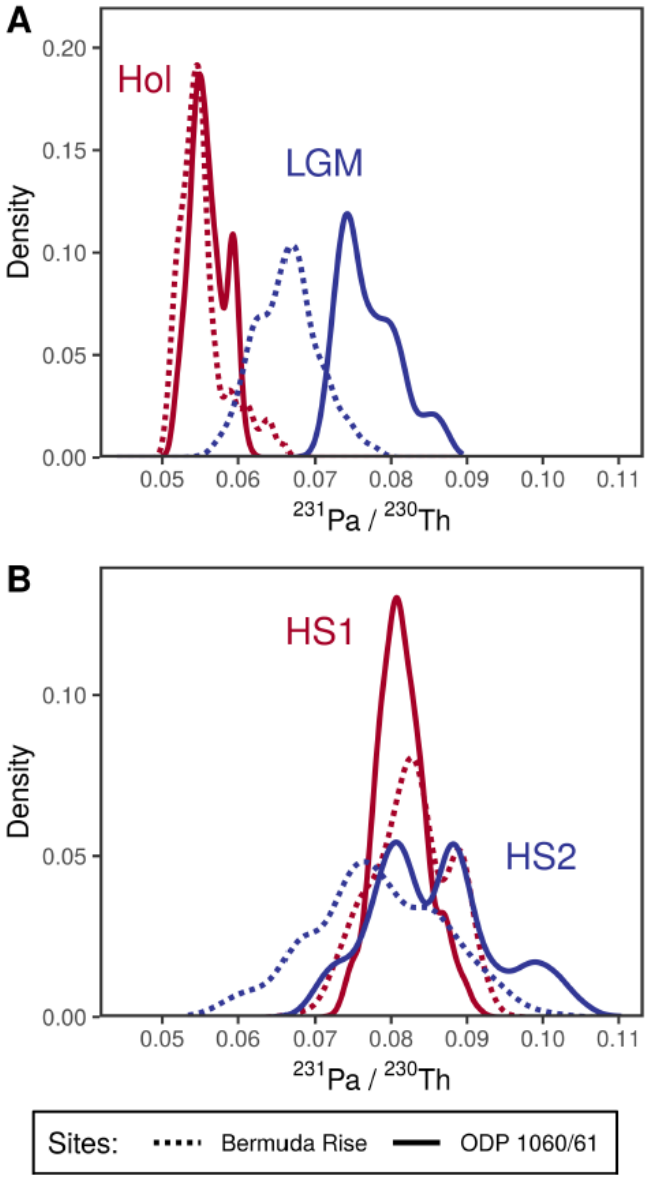

Figure 4: Probability density distribution of $^{231}Pa/^{230}Th$ values measured at Bermuda Rise and Blake Ridge for different time slices. Data from Sites 1060 and 1061 and those from the Bermuda Rise (ODP 1063 and OCE326-GGC5; McManus et al., 2004; Lippold et al., 2009) were each merged to form two separate stacks. Density distributions were calculated assuming normal distributions of the uncertainties in the measured data and combining all available data inside the respective time intervals: Holocene (0 - 8 ka), LGM (19 - 23 ka), HS1 (15 - 18 ka), and HS2 (24 -27 ka). During the Holocene both sites displayed similar $^{231}Pa/^{230}Th$ values (panel A), while the LGM was significantly different. Panel B indicates that values during HS1 and HS2 were analogue during both periods.

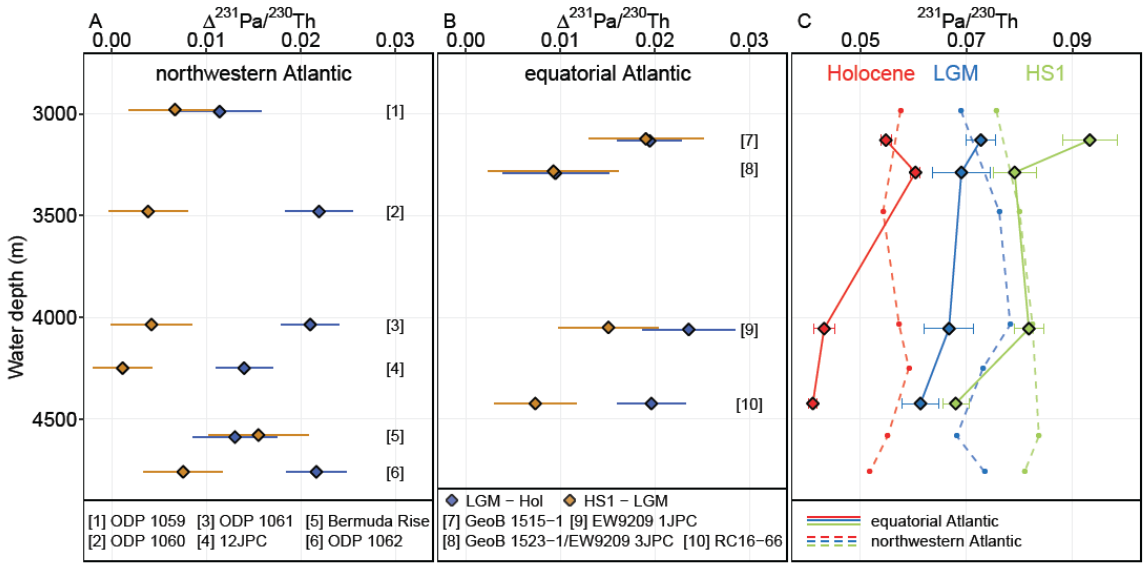

Figure 5: (A,B) $\Delta^{231}Pa/^{230}Th$ (differences of $^{231}Pa/^{230}Th$ between LGM and Holocene (blue) and between HS1 and LGM (brown)) from the northwestern Atlantic (A) and the equatorial Atlantic (B). Horizontal bars indicate errors. Please note, all data in panel A and B plot at positive $\Delta^{231}Pa/^{230}Th$ values indicative of AMOC strengths in the order: Holocene>LGM>HS1. Divergence of individual points of one core site (sites are indicated with the numbers in brackets) indicate the strength of AMOC during the LGM. (C) Depth transect for all sites presented in panel A and B from the equatorial Atlantic (solid line) and the northwestern Atlantic (dashed line; cf. Fig. 3). Depth transects are presented for time slices of the Holocene, LGM and HS1.